Allosteric modulation of β1 integrin function induces lung repair in animal model of emphysema.

Rehab Al-Jamal[1], Linda Wilson[2], Chris J. Armit[1], Susan McIntyre[1], Mark Marsden[4] , Steven D. Shapiro[3], and David J. Harrison[1].

1. Division of Pathology, University of Edinburgh, Cancer Research Centre, Crewe Road South, Edinburgh, EH4 2XR, United Kingdom; 2. School of Biomedical Sciences, Hugh Robson Building, George Square, University of Edinburgh, Edinburgh EH8 9XD, United Kingdom. 3. Department of Medicine, University of Pittsburgh, 1218 Scaife Hall, 3550 Terrace Street, Pittsburgh, PA 15261, USA 4. MRC Centre for Inflammation Research, Queen's Medical Research Institute, University of Edinburgh, 47 Little France Crescent, Edinburgh EH16 4TJ, United Kingdom.

Correspondence should be addressed to R. Al-Jamal (r.al-jamal@ed.ac.uk).

Abstract

Emphysema is a progressive lung disease characterised by loss of lung parenchyma with associated functional changes including decreased tissue elastance. Here we report β1 integrin is a novel target for tissue repair and regeneration in emphysema. We show a single dose of a monoclonal antibody against β1 integrin induced both functional and structural reversal of elastase-induced lung injury *in vivo,* and we found that similar matrix remodelling changes occurred in human lung tissue. We also identified a potential mechanism of action as this allosteric modulation of β1 integrin inhibited elastase-induced caspase activation, F-actin aggregate formation and changes in cellular ATP levels. This was accompanied by maintenance of β1 integrin levels and inhibition of caveolin-1 phosphorylation. We propose that allosteric modulation of β1 integrin-mediated mechanosensing prevents cell death associated with lung injury and progressive emphysema, thus allowing cells to survive and for repair and regeneration to ensue.

Introduction

Chronic Obstructive Pulmonary Disease (COPD) is characterised by poorly reversible and progressive airflow limitation associated with chronic bronchitis and emphysema (1). There are currently no effective treatments for emphysema to halt, slow or reverse the disease (1). Prospective treatments are focussed on the amelioration of the inflammation associated with the disease. The emphasis of our studies has been on the largely unexplored areas of repair and regeneration in emphysema.

Recent paradigms proposed in emphysema pathogenesis include the interaction of apoptosis, oxidative stress and protease/antiprotease imbalance where inflammation is a consequence to cumulative cellular injury (2). The cell responses to such injuries are directed toward cell arrest, or, if the damage is beyond repair, toward cell death (3). This leads to the hypothesis that alveolar cell apoptosis is a critical determinant in the pathogenesis and progression of emphysema; a key observation documented both in human and animal models (4;5). Apoptosis may be induced by physical insult, ligation of receptors, or altered extracellular matrix (ECM) composition and/or attachment.

The ECM interacts with integrins and modifies their function. Integrins are a family of heterodimeric cell surface receptors composed of α and β subunits. There is substantial molecular evidence for the role of integrins in tissue organisation due to their role in cell-ECM and cell-cell adhesion (6;7). These properties give integrins key roles in cell growth, differentiation, migration, and survival. Little is known about the role of β1 integrin specifically in the lung in health and disease, but interestingly, β1 integrin has been implicated in cardiac fibrosis (8) and epithelial proliferation (9).

We questioned whether, in emphysematous lung injury, β1 integrin function is involved in regulation of apoptosis of lung cells, with the corollary that modifiers of integrin function could be therapeutically beneficial. We have established an in vitro model system which replicated features of elastase-induced injury in vivo. Using this system, we identified a novel mechanism of β1 integrin-mediated repair in which allosteric modulation of the receptor inhibited caspase activation, F-actin aggregate formation and fluctuations in cellular ATP levels. This inhibition was obtained under conditions in which the total β1 expression was unchanged and clustering inhibited.

Results

We used several functional monoclonal antibodies, one of which, predicted to modify β1 integrin allostery by binding to the hybrid domain of the receptor, had a marked therapeutic effect. This antibody, JB1a, binds to an epitope within the β1 integrin's hybrid domain irrespective of conformational state of the receptor. Targeting amino acid sequences in this region using antibodies have been reported to stabilise the physiological intermediate state of the receptor in a similar fashion as an allosteric antagonist (10).

Allosteric modulation of β1 integrin increases ECM production

We first investigated whether β1 integrin allosteric modulation altered the ECM, focussing on perlecan because of its known role in basement membrane integrity. In a co-culture of primary human alveolar epithelial cells with lung interstitial cells, the anti-β1 integrin antibody JB1a caused an increase in perlecan (figure 1a); a change that

persisted for 24 hours and was partially sensitive to pre-treatment with cycloheximide and the non-specific MMPs activator aminophenylmercuric acetate (APMA). Treatment with neutralising anti-MMPs 7 and 9 antibodies failed to produce a similar increase in perlecan expression. The changes in perlecan in response to JB1a were accompanied by an increase in tissue inhibitors of metalloproteinase-1 (TIMP1) initially (figure 1b) and pro-MMP-9 subsequently (figure 1c). The results indicate that JB1a-induced changes in proteoglycan are not solely due to alteration in the MMP/TIMP balance. Similar responses in human lung explants and the alveolar cell line, NCI-H441, were also obtained and were specific to JB1a treatment (data not shown). As controls we demonstrated that the anti-β1 integrin antibody TS2/16, which binds the 207-218 amino acid sequence, and 6S6 clone, which binds a discontinuous unmapped epitope, had no effect on proteoglycans.

Allosteric modulation of β1 integrin effects reversal of emphysematous injury in vivo.

In order to investigate whether allosteric modulation of β1 integrin was of therapeutic value, mice were treated with the anti β1 integrin monoclonal antibody, JB1a, or vehicle, either once on day 14 (21 day group, 21d) or on days 21 and 28 (35 day group, 35d) after elastase instillation and the achievement of maximal air space enlargement on the basis of a pilot time course study and previous reports (11). Both JB1a and 6S6 clones bind β1 integrin in mouse tissues (12). We have further confirmed that JB1a binds β1 integrin in murine tissue by immunoprecipitation followed by mass spectrometry and western analyses to ascertain the identity of the protein to which the JB1a clone binds in murine tissues (data not shown). An additional group receiving

elastase and the isotype control IgG1, MOPC21, was performed and showed no reversal of elastase-induced structural damage (data not shown). The clone 6S6 did not induce repair *in vivo* (data not shown). This clone is known to induce aggregation in addition to adhesion blocking.

Allosteric modulation of β1 integrin effects functional reversal of emphysematous injury in vivo.

As expected, there was a marked leftward shift in the respiratory pressure-volume curve (PV) in response to elastase, and there was a progressive increase in the PV shape exponential constant, k, particularly in the 35 day group (figure 2a-b). This shift was reversed by JB1a treatment (figure 2a-b, for 35 day data, 21 day data not shown). Furthermore, the effect of elastase treatment on the peak pressures and quasi-static elastance derived from the PV curves were significantly reversed by JB1a treatment (figures 2c and 2d).

Allosteric modulation of β1 integrin effects structural reversal of emphysematous injury in vivo.

Lung morphometry demonstrated that JB1a treatment also reversed elastase-induced air space enlargement (figures 3a and 3b). The explanation for the discrepancy between the functional and structural differences of the 21day and 35day treatment groups may reflect the presence of inflammation, noted histologically in the 21day but not 35 day group. The functional reversal was accompanied by reversal in elastase-induced damage to elastic fibres (data not shown).

To ascertain the effects of allosteric modulation of β1 integrin on lung structural repair, we assessed the number of contiguous airspaces using image analysis of histological sections from the 21day group (Figure 3c-e, Figure 4 for method). Elastase pre-treatment decreased the number of contiguous airspaces and was reversible by JB1a treatment (Figure 3c). In addition, elastase pre-treatment caused a decrease in the number of septal junctions which was partially reversed by JB1a (Figure 3d). No change was seen in the number of septal ends (Figure 3e).

The effect of allosteric modulation of β1 integrin on alveolar septation

Using 3D image reconstructions of expression pattern of TTF-1 and GATA-6 in 21day group animals, two transcription factors which control septation in the developing lung (13;14) were investigated.

GATA-6 expression demarcates alveolar boundaries, and is increased following elastase-induced injury

Following elastase-induced air space enlargement in the lung in the 21day group, an increase in GATA-6 staining was observed in alveoli in comparison to vehicle-treated animals (Figure 5). JB1a treated animals exhibited a less pronounced GATA-6 staining in comparison to elastase-treated mice (Figure 5). However, the pattern of GATA-6 expression displayed marked differences following antibody treatment in comparison to vehicle-treated mice, as revealed by 3D reconstructions of immunohistochemically-labelled slides. Airspace enlargement was patchy in 21day JB1a-treated lungs (Figure 5) and these were rich in GATA-6 expressing structures, many of which were elongated relative to vehicle-treated controls whereas the non-emphysematous areas displayed punctate GATA-6 structures as in vehicle-treated lungs (Figure 5) and appeared hypercellular (Figure 5) relative to vehicle-treated controls (Figure 5). The patchy

emphysematous regions in JB1a treated lungs (Figure 5) resembled smooth saccular structures not unlike those observed in mouse neonatal lung immediately prior to formation of the secondary septa.

Although varying levels of airspace enlargement (emphysema) were observed in 3D reconstructions of PPE-treated lung with occasional elongated GATA-6 expressing structures (Figure 5), no saccular structures typical of emphysematous regions of JB1a treated lungs were observed.

Hyperplasia of TTF-1 expressing cells is a feature of β1 integrin antibody treatment in elastase-injured lung

In both elastase-injured and vehicle-treated lungs, TTF-1 expression localised to either cells residing in the corner of the alveolus or at the free septal end (Figure 5). 3D reconstructions revealed that TTF-1 expressing cells often appeared in clusters in all 21 day groups albeit the expression patterns in elastase-injured lungs (Figure 5) were similar to those of vehicle-treated lungs (Figure 5). By contrast, a marked hyperplasia of TTF-1 expressing cells was observed in antibody-treated lungs in both emphysematous (Figure 5) and non-emphysematous areas (Figure 5).

By assessing the co-distribution of GATA-6 and TTF-1 in 3D reconstructions, it was determined that areas of TTF-1 cell hyperplasia (Figure 5) did not co-localise with GATA-6 expression but rather appeared adjacent. Thus, it would appear that in the lung, GATA-6 and TTF-1 have discrete expression domains.

Allosteric modulation of β1 integrin reduced cell death after emphysematous injury in vivo.

Allosteric modulation of β1 integrin affects both mitosis (15) and cell death (16). Since cell death has been implicated in COPD progression (5;17), we evaluated the prevalence of TUNEL positive cells in mouse lung at days 21 and 35 following injury with or without JB1a treatment. There was a significant increase in TUNEL positive cells in the lung both at 21 days and 35 days post-elastase instillation: this was significantly reduced by subsequent treatment with JB1a (figures 6a and b).

The cellular mechanism of reversal of emphysema using an in vitro system induced by β1 integrin allosteric modulation.

Elastase can induce apoptosis of epithelial cells secondary to altered attachment (anoikis), accompanied by alteration in mitochondrial permeability and caspase activation (18). In a co-culture of adult human lung fibroblasts over-layered with NCI-H441 cells, under cyclic mechanical stimulation, we show that elastase treatment caused a significant increase in caspase 3 and 7 activity, consistent with previous reports (19). Addition of JB1a to the cultures inhibited elastase-induced caspase activation in a similar fashion to the broad spectrum caspase inhibitor, ZVAD-fmk (figure 7a).

Furthermore, we found that elastase treatment increased F-actin aggregates, changes inhibited by both JB1a and ZVAD-fmk (figure 7b). In time lapse studies and 3D reconstructions, we were able to demonstrate the increase in de novo F-actin formation during the course of elastase-induced injury which was followed by activation of caspase 3 and 7 (Figure 7c, for movies see supplementary online data).

Formation of F-actin from monomeric G-actin is energy dependent and under ATP depletion conditions, there is a net conversion of monomeric G-actin to polymeric F-

actin. We measured ATP levels in co-cultures in response to elastase and JB1a. Elastase reduced the levels of ATP, a response inhibited by JB1a (figure 8). Of note is also the amplitude of fluctuations in ATP level in response to elastase, a pattern attenuated by JB1a.

β1 integrin-mediated adhesion has been shown to regulate cholesterol-rich membrane microdomain internalisation mediated by phospho-caveolin-1 (20). In co-cultures, elastase significantly reduced cell membrane-associated β1 integrin levels (figure 9a) and induced phosphorylation of caveolin-1 within two hours; changes inhibited by JB1a (figure 9b-c).

Discussion

In this report we have investigated the role of β1 integrin in lung repair in emphysema. We questioned whether β1 integrin becomes allosterically activated in epithelial or mesenchymal cells, with the corollary that allosteric antagonists could be therapeutically beneficial. The key finding of our investigation was that by direct allosteric modulation of β1 integrin with a single dose of monoclonal antibody, both functional and structural reversal of elastase-induced tissue injury were induced *in vivo*. This effect appeared to be due to increase septation. We further demonstrate a potential cellular mechanism for this β1 integrin-mediated repair. In order to do so, we established an in vitro model system which replicated features of elastase-induced emphysema in vivo. We identified that allosteric modulation of β1 integrin inhibited caspase activation, F-actin aggregate formation and fluctuations in cellular ATP levels, under conditions in which the total β1 expression was changed and clustering inhibited.

Our findings support the notion that cytomechanics are important determinants of cell fate (21) and effect repair (22).

So the intriguing question is what is the role of β1 integrin within the context of remodelling. Previous reports demonstrated that excision of β1 integrin gene in cardiac myocytes resulted in postnatal cardiac fibrosis, depressed cardiac function and increased myocardial glucose metabolism leading to spontaneous heart failure (8). Conditional deletion of β1 integrin in the intestinal epithelium of mice causes a significant increase in epithelial proliferation without affecting cell adhesion (23).

It is important to note that although the knock-out or transgenic approaches have highlighted the crucial role for β1 integrin, they do not elucidate more subtle functions, such as those controlled by avidity regulation. Integrins in general, including β1 integrin, are known to exhibit global structural rearrangement and exposure of ligand binding sites upon activation (24). The overall strength of cellular adhesiveness or avidity is governed by affinity and valency; the latter governed by the density of the receptor and its ligand on the cell surface as well as the spatial and geometric arrangement and movement (24;25). Overall, integrin have three possible conformations of the extracellular domain; a low affinity bent conformation, an extended conformation with closed headpiece representing an intermediate affinity state, and the ligand-binding induced high affinity extended form with an open headpiece (26). Current integrin antagonists fall into three classes; direct inhibitors of ligand binding to the I domain of the α chain, allosteric inhibitors of the I domain of the α chain and allosteric antagonists of α chain/β I-like domains (25).

The expression of activation epitopes of β1 integrin, and hence a fully extended active conformation, is present in asthmatic patients and correlates with airway hyper-responsiveness (27). Full activation of β1 integrin is required for MMP activation (7), an important component during remodelling. However, a function modifying antibody which induces an allosteric modulation locking the receptor in an intermediary low affinity physiological state increased proliferation in human mammary epithelial cells (28).

We also questioned how allosteric modulation promoted structural repair in emphysematous lungs. The two main events in lung morphogenesis are branching of the conducting airways and alveolar septation. In emphysema, the complexity of individual alveoli is lost. Additionally, it is known that the formation of new septa slows with advancing age, and it is feasible that emphysema in the adult may reflect a defect in septation. Alveolar septation is regulated by transcription factors such as GATA-6 and TTF-1 (29;30). Septation involves the subdivision of the large, primitive airspace via the budding of type II progenitor cells from the primary septa into the alveolar space. These new secondary septa may meet with one another before differentiating into the thin, squamous type I epithelial cells typical of mature septa (31;32). By virtue of their importance during alveolarisation in the postnatal lung, it is possible that the expression levels of GATA-6 and TTF-1 may highlight restrictions on new septa formation in adult lung. To address this issue, we employed image processing techniques including 3D reconstructions of TTF-1 and GATA-6 expression patterns and automated stereological counting methods as a means of assessing whether there is a relationship between the expression of these transcription factors and the incidence of septation in after elastse-induced injury. We demonstrated that GATA-6 expression is increased following elastase-injury and associates with a decrease in the number of alveolar septal junctions and contiguous airspaces. In addition, allosteric modulation of β1 integrin induced a marked hyperplasia of TTF-1 expressing cells, and attenuated the GATA-6 upregulation

associated with elastase-injury. GATA-6 regulates differentiation of the alveolar type II cell, and may distinguish an intermediate cell type with characteristics of both the type II and type I cell (33). Our observation that GATA-6 is highly expressed in the thickened septa that surround enlarged airspaces in antibody-treated lungs is consistent with this possibility, and may reflect epithelial cells in the process of differentiating from type II to type I cells. However, it is additionally possible that the existence of these thick, cable-like cells highlights a possible failure of septal cells to differentiate into thin, type I cells in emphysematous areas. It has been recently suggested that newly transdifferentiated cells in the lung are more prone to cell death and may be a mechanism for limiting physiologic repair after injury (34). Notwithstanding this, it is noteworthy that in all instances GATA-6 was expressed in only a portion of alveolar epithelial cells, and that these were not connected with one another.

Analysis of TTF-1 in vehicle-treated lungs revealed that TTF-1 was expressed in alveolar corner cells and cells of the free septal ends. The former are most likely type II epithelial cells whereas the latter may reflect type II cells in the process of transdifferentiating into myofibroblasts (34-36). Epithelial-mesenchymal transitions are a feature of the alveolus and it is feasible that the type II cell may migrate to a free septal end whereby it differentiates into a myofibroblast. The myofibroblast, committed to ECM deposition and tissue repair, may present as a considerable boon to a remodelling alveolus. 3D reconstructions revealed that TTF-1 expression patterns in elastase-injured lungs were similar to those of vehicle-treated lungs. By contrast, the number of TTF-1 expressing cells increased following antibody treatment and 3D reconstructions revealed a marked hyperplasia of TTF-1 expressing cells in both emphysematous and repaired regions. These findings suggest that modulating β1 integrin function allows septation to proceed in damaged lungs by altering the pool of GATA-6 and TTF-1 expressing cells.

On the basis of these findings and the *in vivo* TUNEL data, we investigated the cellular mechanism of epithelial-mesenchymal response to emphysematous injury *in vitro.* Butler and colleagues reported that ligand or antibody-induced activation and/or clustering of integrins promotes actin polymerisation in a dose-dependent manner (19). Changes in cytomechanics is a determinant of cell fate (21;37). Evidence that F-actin aggregates are involved in cellular injury leading to death comes from studies where cisplatin-induced loss of cell-cell contacts was associated with the increased formation of F-actin stress fibres and subsequently apoptosis (38). Changes in actin dynamics also affect mitochondrial function and release of reactive oxygen species eliciting death signals (reviewed in detail in (39)). Retro-retinoids (a metabolite of retinol) trigger apoptosis mediated by F-actin aggregate formation (40). Indeed, several serine proteases including elastase have been shown to decrease mitochondrial membrane potential, release of cytochrome c to the cytosol, and cleavage of caspases-9 and -3 in both lung fibroblasts and bronchial epithelial cells (18;41;42). Lipopolysaccharide has been reported to increase integrin function and cell-matrix adhesion, leading to impaired enterocyte migration in necrotizing enterocolitis (18;43).

We have found that in our in vitro epithelial mesenchymal cultures, elastase induced caspase activation. The effect was accompanied by an increase in F-actin. The live cell imaging provides a stronger evidence of de novo increase in the formation of actin aggregates since the phalloidin staining fails to demonstrate the newly formed aggregate. We used an experimental strategy in which cells were loaded with labelled monomeric actin just prior to the onset of injury. Furthermore, we were able to show caspase activation in real-time. Both, elastase-induced caspase activation and actin aggregate formation were inhibited by the allosteric modulation of β1 integrin. Under ATP depletion conditions, there is a net conversion of monomeric G-actin to polymeric F-actin resulting from an alteration in the ratio of ATP-G-actin and ADP-G-actin with the resultant F-actin forming dispersed aggregates. Actin polymerisation consumes 50%

of total cellular ATP. We chose to characterise ATP dynamic changes in vitro following elastase induced-injury. We found not only the levels were reduced after prolonged exposure but preceding this reduction, abnormal fluctuations were detected at the onset of exposure to elastase. These responses were inhibited by allosteric modulation of β1 integrin. Recent report has indicated that the addition of ATP to lung epithelial cells inhibited injury (44).

Recent reports have shown that the administration of β4 thymosin, an actin-sequestering protein, promoted cardiac repair after ischemia-reperfusion injury (22). Additionally, gene disruption of caveolin-1, which is known to be involved in integrin clustering and activation, results in pulmonary fibrosis and impairment in liver regeneration after partial hepatectomy which was reversible by treatment with glucose (45), indicating the probable importance of energy preservation. Furthermore, Bhatia et al. proposed that abnormal integrin-cytoskeletal interaction restricts the mobility of integrin receptors and results in defective integrin function (46), and that the Abi1 pathway is required for Bcr-Abl to stimulate actin cytoskeleton remodelling, integrin clustering and cell adhesion (47). Interestingly, previous reports have shown that β1 integrin-mediated adhesion regulate cholesterol-rich membrane microdomain internalisation mediated by phospho-caveolin-1 (48) and caveolar endocytosis can be blocked by small interfering RNA knockdown of β1 integrin (49). Our findings that allosteric modulation inhibits elastase-induced caveolin phosphorylation reinforces the idea that, in injury, abnormal integrin activation, clustering and the resulting changes in the cytoskeleton could be key to cellular damage in emphysema.

In conclusion, we propose that elastase-induced progressive damage is partly due to anoikis resulting from an increase in cytoskeletal tension caused by increased actin polymerisation, rendering the cell rigid and susceptible to physiological forces.

More importantly, we have shown for the first time the potential therapeutic effect of allosteric modulation of β1 integrin in tissue repair in emphysema. We suggest a paradigm for the pathogenesis and treatment of emphysema based upon β1 integrin and its effect on cell survival, mediated by alteration of adhesion and cytoskeletal tethering and energy preservation. We propose that an initial insult changes the mechanical tethering of cells to ECM, perhaps due to ECM degradation (50) thus changing cell mechanosensing, leading to ATP depletion and eventual cell death.

Acknowledgments. The authors also wish to thank Robert J. Naylor for the scientific and editorial guidance and James G. Martin for his valuable scientific advice. We would also like to thank William H. Wallace for assistance in obtaining the human lung tissues. We are indebted to Bernard Ramsahoye for critical evaluation of the manuscript. This work was supported in part by a Pathology Endowment Fund and the Chief Scientist Office, Scottish Executive.

Competing Interests Statement Rehab Al-Jamal and David Harrison are the inventors for the intellectual property detailing the therapeutic effects of the modulation of β1 integrin function.

Authors' Contributions statement Rehab Al-Jamal and David Harrison contributed to the intellectual property, scientific input, planning and carrying out the experiments of the project. Linda Wilson participated in the confocal imaging and time lapse experiments in the investigation of mechanisms of injury and repair. Christopher J. Armit performed the 3d analyses and immunostaining of TTF1 and GATA6 from the in vivo studies. Steven D. Shapiro has provided critical appraisal and discussion of the scientific aspects of the mechanisms of β1 integrin-mediated repair. Susan McIntyre performed the ATP experiments. Mark Marsden has provided technical help with establishing the preliminary proof-of-concept experiment to validate the therapeutic effect of the JB1a antibody.

Reference List

1. Al Jamal,R., Wallace,W.A., and Harrison,D.J. 2005. Gene therapy for chronic obstructive pulmonary disease: twilight or triumph? *Expert.Opin.Biol.Ther.* 5:333-346.
2. Tuder,R.M., Yoshida,T., Arap,W., Pasqualini,R., and Petrache,I. 2006. State of the Art. Cellular and Molecular Mechanisms of Alveolar Destruction in Emphysema: An Evolutionary Perspective. *Proc Am Thorac Soc* 3:503-510.
3. Barabasi,A.L. and Bonabeau,E. 2003. Scale-free networks. *Sci.Am* 288:60-69.
4. Segura-Valdez,L., Pardo,A., Gaxiola,M., Uhal,B.D., Becerril,C., and Selman,M. 2000. Upregulation of Gelatinases A and B, Collagenases 1 and 2, and Increased Parenchymal Cell Death in COPD. *Chest* 117:684-694.
5. Petrache,I., Natarajan,V., Zhen,L., Medler,T.R., Richter,A.T., Cho,C., Hubbard,W.C., Berdyshev,E.V., and Tuder,R.M. 2005. Ceramide upregulation causes pulmonary cell apoptosis and emphysema-like disease in mice. *Nat.Med.* 11:491-498.
6. Levkau,B., Kenagy,R.D., Karsan,A., Weitkamp,B., Clowes,A.W., Ross,R., and Raines,E.W. 2002. Activation of metalloproteinases and their association with integrins: an auxiliary apoptotic pathway in human endothelial cells. *Cell Death.Differ.* 9:1360-1367.
7. Festuccia,C., Angelucci,A., Gravina,G., Eleuterio,E., Vicentini,C., and Bologna,M. 2002. Bombesin-dependent pro-MMP-9 activation in prostatic cancer cells requires beta1 integrin engagement. *Exp.Cell Res.* 280:1-11.
8. Shai,S.Y., Harpf,A.E., Babbitt,C.J., Jordan,M.C., Fishbein,M.C., Chen,J., Omura,M., Leil,T.A., Becker,K.D., Jiang,M. *et al*. 2002. Cardiac Myocyte-Specific Excision of the {beta}1 Integrin Gene Results in Myocardial Fibrosis and Cardiac Failure. *Circ Res* 90:458-464.

9. Jones,R.G., Li,X., Gray,P.D., Kuang,J., Clayton,F., Samowitz,W.S., Madison,B.B., Gumucio,D.L., and Kuwada,S.K. 2006. Conditional deletion of {beta}1 integrins in the intestinal epithelium causes a loss of Hedgehog expression, intestinal hyperplasia, and early postnatal lethality. *J Cell Biol.* 175:505-514.
10. Luo,B.H., Strokovich,K., Walz,T., Springer,T.A., and Takagi,J. 2004. Allosteric beta1 integrin antibodies that stabilize the low affinity state by preventing the swing-out of the hybrid domain. *J.Biol.Chem.* 279:27466-27471.
11. Lucey,E.C., Goldstein,R.H., Breuer,R., Rexer,B.N., Ong,D.E., and Snider,G.L. 2003. Retinoic acid does not affect alveolar septation in adult FVB mice with elastase-induced emphysema. *Respiration* 70:200-205.
12. Cavallaro,U., Niedermeyer,J., Fuxa,M., and Christofori,G. 2001. N-CAM modulates tumour-cell adhesion to matrix by inducing FGF-receptor signalling. *Nat.Cell Biol.* 3:650-657.
13. Korfhagen,T.R. and Whitsett,J.A. 1997. Transcriptional control in the developing lung. The Parker B. Francis lectureship. *Chest* 111:83S-88S.
14. Liu,C., Ikegami,M., Stahlman,M.T., Dey,C.R., and Whitsett,J.A. 2003. Inhibition of alveolarization and altered pulmonary mechanics in mice expressing GATA-6. *Am.J Physiol Lung Cell Mol.Physiol* 285:L1246-L1254.
15. Reverte,C.G., Benware,A., Jones,C.W., and LaFlamme,S.E. 2006. Perturbing integrin function inhibits microtubule growth from centrosomes, spindle assembly, and cytokinesis. *J Cell Biol.* 174:491-497.
16. Nakayamada,S., Saito,K., Fujii,K., Yasuda,M., Tamura,M., and Tanaka,Y. 2003. beta1 integrin-mediated signaling induces intercellular adhesion molecule 1 and Fas on rheumatoid synovial cells and Fas-mediated apoptosis. *Arthritis Rheum.* 48:1239-1248.

17. Tsuji,T., Aoshiba,K., and Nagai,A. 2006. Alveolar cell senescence in patients with pulmonary emphysema. *Am.J Respir.Crit Care Med.* 174:886-893.

18. Suzuki,T., Moraes,T.J., Vachon,E., Ginzberg,H.H., Huang,T.T., Matthay,M.A., Hollenberg,M.D., Marshall,J., McCulloch,C.A., Abreu,M.T. *et al*. 2005. Proteinase-activated receptor-1 mediates elastase-induced apoptosis of human lung epithelial cells. *Am.J.Respir.Cell Mol.Biol.* 33:231-247.

19. Butler,B., Gao,C., Mersich,A.T., and Blystone,S.D. 2006. Purified integrin adhesion complexes exhibit actin-polymerization activity. *Curr.Biol.* 16:242-251.

20. del Pozo,M.A., Balasubramanian,N., Alderson,N.B., Kiosses,W.B., Grande-Garcia,A., Anderson,R.G., and Schwartz,M.A. 2005. Phospho-caveolin-1 mediates integrin-regulated membrane domain internalization. *Nat.Cell Biol.* 7:901-908.

21. Chen,C.S., Mrksich,M., Huang,S., Whitesides,G.M., and Ingber,D.E. 1997. Geometric control of cell life and death. *Science* 276:1425-1428.

22. Bock-Marquette,I., Saxena,A., White,M.D., Dimaio,J.M., and Srivastava,D. 2004. Thymosin beta4 activates integrin-linked kinase and promotes cardiac cell migration, survival and cardiac repair. *Nature* 432:466-472.

23. Jones,R.G., Li,X., Gray,P.D., Kuang,J., Clayton,F., Samowitz,W.S., Madison,B.B., Gumucio,D.L., and Kuwada,S.K. 2006. Conditional deletion of {beta}1 integrins in the intestinal epithelium causes a loss of Hedgehog expression, intestinal hyperplasia, and early postnatal lethality. *J Cell Biol.* 175:505-514.

24. Carman,C.V. and Springer,T.A. 2003. Integrin avidity regulation: are changes in affinity and conformation underemphasized? *Curr.Opin.Cell Biol.* 15:547-556.

25. Shimaoka,M. and Springer,T.A. 2003. Therapeutic antagonists and conformational regulation of integrin function. *Nat.Rev.Drug Discov.* 2:703-716.

26. Xiao,T., Takagi,J., Coller,B.S., Wang,J.H., and Springer,T.A. 2004. Structural basis for allostery in integrins and binding to fibrinogen-mimetic therapeutics. *Nature* 432:59-67.

27. Johansson,M.W., Barthel,S.R., Swenson,C.A., Evans,M.D., Jarjour,N.N., Mosher,D.F., and Busse,W.W. 2006. Eosinophil beta 1 integrin activation state correlates with asthma activity in a blind study of inhaled corticosteroid withdrawal. *J.Allergy Clin.Immunol.* 117:1502-1504.

28. Seewaldt,V.L., Mrozek,K., Sigle,R., Dietze,E.C., Heine,K., Hockenbery,D.M., Hobbs,K.B., and Caldwell,L.E. 2001. Suppression of p53 function in normal human mammary epithelial cells increases sensitivity to extracellular matrix-induced apoptosis. *J Cell Biol.* 155:471-486.

29. Liu,C., Morrisey,E.E., and Whitsett,J.A. 2002. GATA-6 is required for maturation of the lung in late gestation. *Am J Physiol Lung Cell Mol.Physiol* 283:L468-L475.

30. Wert,S.E., Dey,C.R., Blair,P.A., Kimura,S., and Whitsett,J.A. 2002. Increased expression of thyroid transcription factor-1 (TTF-1) in respiratory epithelial cells inhibits alveolarization and causes pulmonary inflammation. *Dev.Biol.* 242:75-87.

31. Takaro,T., Parra,S.C., and Peduzzi,P.N. 1985. Anatomical relationships between type II pneumonocytes and alveolar septal gaps in the human lung. *Anat.Rec.* 213:540-550.

32. Oldmixon,E.H., Butler,J.P., and Hoppin,F.G., Jr. 1989. Lengths and topology of alveolar septal borders. *J Appl.Physiol* 67:1930-1940.

33. Keijzer,R., van Tuyl,M., Meijers,C., Post,M., Tibboel,D., Grosveld,F., and Koutsourakis,M. 2001. The transcription factor GATA6 is essential for branching morphogenesis and epithelial cell differentiation during fetal pulmonary development. *Development* 128:503-511.

34. Kim,K.K., Kugler,M.C., Wolters,P.J., Robillard,L., Galvez,M.G., Brumwell,A.N., Sheppard,D., and Chapman,H.A. 2006. Alveolar epithelial cell mesenchymal

transition develops in vivo during pulmonary fibrosis and is regulated by the extracellular matrix. *Proc.Natl.Acad.Sci U.S.A* 103:13180-13185.

35. Yao,H.W., Xie,Q.M., Chen,J.Q., Deng,Y.M., and Tang,H.F. 2004. TGF-beta1 induces alveolar epithelial to mesenchymal transition in vitro. *Life Sci.* 76:29-37.
36. Willis,B.C., Liebler,J.M., Luby-Phelps,K., Nicholson,A.G., Crandall,E.D., du Bois,R.M., and Borok,Z. 2005. Induction of epithelial-mesenchymal transition in alveolar epithelial cells by transforming growth factor-beta1: potential role in idiopathic pulmonary fibrosis. *Am J Pathol.* 166:1321-1332.
37. Ingber,D.E. 2002. Mechanical signaling and the cellular response to extracellular matrix in angiogenesis and cardiovascular physiology. *Circ.Res.* 91:877-887.
38. Imamdi,R., de Graauw,M., and van de,W.B. 2004. Protein kinase C mediates cisplatin-induced loss of adherens junctions followed by apoptosis of renal proximal tubular epithelial cells. *J.Pharmacol.Exp.Ther.* 311:892-903.
39. Gourlay,C.W. and Ayscough,K.R. 2005. The actin cytoskeleton: a key regulator of apoptosis and ageing? *Nat.Rev.Mol.Cell Biol.* 6:583-589.
40. Korichneva,I. and Hammerling,U. 1999. F-actin as a functional target for retro-retinoids: a potential role in anhydroretinol-triggered cell death. *J.Cell Sci.* 112 (Pt 15):2521-2528.
41. Aoshiba,K., Yasuda,K., Yasui,S., Tamaoki,J., and Nagai,A. 2001. Serine proteases increase oxidative stress in lung cells. *Am.J.Physiol Lung Cell Mol.Physiol* 281:L556-L564.
42. Ginzberg,H.H., Shannon,P.T., Suzuki,T., Hong,O., Vachon,E., Moraes,T., Abreu,M.T., Cherepanov,V., Wang,X., Chow,C.W. *et al*. 2004. Leukocyte elastase induces epithelial apoptosis: role of mitochondial permeability changes and Akt. *Am.J.Physiol Gastrointest.Liver Physiol* 287:G286-G298.

43. Qureshi,F.G., Leaphart,C., Cetin,S., Li,J., Grishin,A., Watkins,S., Ford,H.R., and Hackam,D.J. 2005. Increased expression and function of integrins in enterocytes by endotoxin impairs epithelial restitution. *Gastroenterology* 128:1012-1022.

44. Lee,B., Rasmussen,D.L., Wang,S.H., Lee,W.Y., Mullon,J.J., Stroetz,R.W., Walters,B.J., and Hubmayr,R.D. 2007. Effects of Osmotic Stress on Alveolar Epithelial Cell Deformation Injury and Repair. *Am.J Respir.Crit Care Med.* 175:A122 (Abstr.)

45. Fernandez,M.A., Albor,C., Ingelmo-Torres,M., Nixon,S.J., Ferguson,C., Kurzchalia,T., Tebar,F., Enrich,C., Parton,R.G., and Pol,A. 2006. Caveolin-1 is essential for liver regeneration. *Science* 313:1628-1632.

46. Bhatia,R., Munthe,H.A., and Verfaillie,C.M. 1999. Role of abnormal integrin-cytoskeletal interactions in impaired beta1 integrin function in chronic myelogenous leukemia hematopoietic progenitors. *Exp.Hematol.* 27:1384-1396.

47. Li,Y., Clough,N., Sun,X., Yu,W., Abbott,B.L., Hogan,C.J., and Dai,Z. 2007. Bcr-Abl induces abnormal cytoskeleton remodeling, beta1 integrin clustering and increased cell adhesion to fibronectin through the Abl interactor 1 pathway. *J Cell Sci.* 120:1436-1446.

48. del Pozo,M.A., Balasubramanian,N., Alderson,N.B., Kiosses,W.B., Grande-Garcia,A., Anderson,R.G., and Schwartz,M.A. 2005. Phospho-caveolin-1 mediates integrin-regulated membrane domain internalization. *Nat.Cell Biol.* 7:901-908.

49. Singh,R.D., Holicky,E.L., Cheng,Z.J., Kim,S.Y., Wheatley,C.L., Marks,D.L., Bittman,R., and Pagano,R.E. 2007. Inhibition of caveolar uptake, SV40 infection, and beta1-integrin signaling by a nonnatural glycosphingolipid stereoisomer. *J Cell Biol.* 176:895-901.

50. Houghton,A.M., Quintero,P.A., Perkins,D.L., Kobayashi,D.K., Kelley,D.G., Marconcini,L.A., Mecham,R.P., Senior,R.M., and Shapiro,S.D. 2006. Elastin

fragments drive disease progression in a murine model of emphysema. *J.Clin.Invest* 116:753-759.

Figure Legends

Figure 1. The effect of allosteric modulation of β1 integrin using JB1a on metalloproteinases and tissue inhibitors of metalloproteinases (MMPs) in primary human lung alveolar/mesenchymal co-cultures. a. shows the effect of JB1a on MMP1 levels and activity at two different time points when added alone and in the presence of APMA, cyloheximide (CXH), neutralising antibodies against MMPs 7 and 9 and broad spectrum MMP inhibitor. b. demonstrates the effects JB1a on tissue inhibitor of metalloproteinase-1 (TIMP1). c. shows the effect of JB1a on the levels of inactive MMP9 (pro-MMP9). The experiment was repeated 3 times using cells derived from different patients.

Figure 2. The effect of porcine pancreatic elastase (PPE) on respiratory function in mice and its reversal using the anti-β1 integrin antibody JB1a. a. the effect of PPE on mean respiratory pressure-volume curves in mice 35 days (35d) after instillation and its reversal by JB1a (JB) (Vehicle=Veh). b. Reversal of PPE-induced increase in the constant k by JB1a treatment at different time points post injury. JB1a treatment once or twice following PPE-induced injury reversed the time-dependent effect on (c) peak respiratory pressure from the pressure-volume curves and (d) the quasi-static elastase derived from a. n=5-6 in 35d groups and n=10 in 21d groups.

Figure 3. The effect of PPE on lung structure and its reversal by JB1a treatment. a. Haematoxylin and eosin staining of lung sections from veh, PPE and JB instilled mice from 21d and 35d groups. b. Mean linear intercept (MLI) measurements from the 21d and 35d groups. Automated stereological estimates of the number of (c) contiguous airspaces, (d) septal junctions, and (e) septal ends from the 21 day group (n=5).

Figure 4. Automated image processing of the septal junctions, septal ends, and contiguous airspaces in the pulmonary acinus in the 21 day group. (1a-c) RGB images from JB (a) PPE (b), and veh lungs (c) were preprocessed with morphological filters (d-f) to aid automated edge detection and to remove noise. (g-i) A 200mm x 200mm frame was superimposed over preprocessed images. Only events completely inside the frame or intersecting the two inclusion edges (South-West boundaries) are considered and any event intersecting the exclusion lines (North-East boundaries) is not sampled. The number of contiguous airspaces (g-i, red), septal branches (j-l, white dots), and free septal ends (m-o, white dots) was determined in reticulin-stained sections of lung.

Figure 5. The effect of allosteric modulation of β1 integrin GATA-6 and TTF-1 expression after PPE-induced. a. 3D reconstructions of PPE-injured lung in the 21 day group of lung parenchyma (blue, Column I), and the expression patterns of GATA-6 (yellow) and TTF-1 (red, Column II). Column III: An overlay of parenchyma and expression patterns of GATA-6 and TTF-1. Column IV: Detail of (Column I) at higher magnification. Column V: Detail of (Column II) at higher magnification.

Figure 6. a. TUNEL staining of lung tissue sections from 21d and 35d group demonstrating the effect of JB1a treatment after PPE-induced lung injury. b. quantification of TUNEL positive cells following PPE-induced injury and JB1a treatment. n=5-6 per group.

Figure 7. The effects of PPE-induced injury and JB1a treatment on (a) capase levels, (b) F-actin and (c) 3D reconstruction of images of human lung co-culture after injury using elastase (b, 0.6 U/ml) demonstrating the formation of F-actin (blue) and caspase

3/7 activation (red). (Ganglioside GM1 for the cell membrane-green) and its inhibition by JB1a (c, 2μg/ml). Vehicle (a)

Figure 8. The effects of PPE-induced injury and JB1a treatment on ATP levels in vitro using human lung co-culture during with mechanical stretch for 6 hours.

Figure 9. The effects of PPE-induced injury alone and in the presence of JB1a treatment on (b) β1 integrin (c) caveolin-1 and (d) phosphorylated caveolin-1 levels in membrane fractions. Representative blots from n=4. Loading controlled by total amount of protein before gradient separation.

Supplementary Material. Time-lapse movies showing the effect of vehicle (a) elastase (b, 0.6 U/ml) on F-actin (blue) and caspase 3/7 activation (red) in vitro using human lung co-culture during mechanical stretch and its inhibition by JB1a (c, 2 μg/ml). Syto 16-green. A figure of the select frames from the recording is provided for the initial submission.

Methods.

Human lung explant culture and human lung cell isolation Human lung tissue specimens were obtained (and approved by NHS ethics committee and with consent) and cultured as either 20-30 mg explant strips or cells. Alveolar epithelial cells were isolated as described before (Elbert et. al., 1999 and Murphy et al., 1999). The cells were then plated onto Transwells of 0.3um pore size (Sigma) and maintained in culture using 1:1 DMEM/F12:Small airway growth media (Cambrex BioScience Wokingham Ltd.) containing 1% fetal calf serum. The remaining tissue was treated with DMEM containing 40% fetal calf serum to inactivate the digestive enzymes and then washed using HEPES buffer. To isolate fibroblasts and smooth muscle cell populations, the tissue was then incubated in DMEM containing 1mg/ml collagenase, 0.5% trypsin and 200U/g DNAsI and maintained at 5% in an CO_2 incubator. The cell suspension was washed as above and cells seeded on multiwell culture plates and maintained in DMEM containing 10% fetal calf serum.

Cultures were subjected to serum starving overnight in a medium containing 0.1% fetal calf serum. Some collagenase digested plated cells were co-cultured with isolated alveolar epithelial cells Transwells at the time of commencing the starvation.

Functional modifying antibody against β1 integrin (Chemicon, clone JB1a, IgG1) was added to the cultures at a concentration of 1.44 and 0.48 μg/ml. The β1 integrin stimulatory antibody clone TS2/16 (IgG1) was also added at 0.9 μg/ml for 1 hour to demonstrate the specificity of the JB1a action. After antibody addition to the cells in culture, the medium was aspirated and the cell layer rinsed twice with ice-cold PBS. The media was aspirated and preserved after the addition of protease inhibitors at –

80^{o}C. In additional experiments, the effect of protein synthesis inhibition on β1 integrin mediated proteoglycan increase was tested by pretreating the human lung derived cells with 25μM cycloheximide. The effect of non-specific activation of metalloproteinases on β1 integrin mediated proteoglycan increase was tested by pretreating the human lung derived cells with 0.5M APMA (aminophenylmercuric acetate). To investigate the involvement of selected metalloproteinases in initiating the response observed with β1 integrin, specific neutralising antibodies for metalloproteinase-7 (1:1000, goat IgG, R&D systems) and metalloproteinase-9 (1:1000 of clone 6-6B, mouse IgG1, Oncogene Research Products) were used. A broad spectrum inhibitor of metalloproteinases was also used at 2.3nM (metalloproteinase inhibitor III, Calbiochem).

SDS-PAGE was also used to separate the denatured proteoglycan and proteins from the tissue concentrated tissue culture supernatants. Perlecan antibody immunoreactive to non-degraded forms of perlecan was used (7B5, mouse IgG1, Zymed Laboratories). metalloproteinase-1 (clone 41-1E5, IgG2a against amino acids 332-350 of human metalloproteinase-1), inactive metalloproteinase-9 (clone 7-11C, mouse IgG1) and TIMP1 (clone 7-6C1, mouse IgG1) antibodies were all from Oncogene Research Products.

PPE-induced air space enlargement model in mice. Female C57/BL6 mice (6-8 weeks old) were instilled intra-tracheally with porcine pancreatic elastase as detailed before (11). All procedures were approved by the UK Home Office and the Institutional Ethics Committee. At day 14 or 21, mice were treated intra-tracheally with the anti-integrin antibody JB1a at 3mg/kg in sterile PBS. The dose chosen is equivalent to the dose of clinically used antibodies against α4β1 integrin (Miller DH, et al. 2003).

Control group was instilled initially with PBS and at day 14 or 21 with PBS. For the group treated at day 14, the animals were terminated at day 21 as follows: The animals were anaesthetised using sodium pentobarbitone (45mg/kg), paralysed using pancuronium bromide (0.8mg/kg) and tracheostomised and ventilated using a small animal ventilator (Flexivent, SCIREQ, Montreal) at 8ml/kg and a rate of 150 breaths/minute and positive end expiratory pressures (PEEP) of 3.5 cmH_2O.

The pressure-volume curve was obtained during inflation and deflation in a stepwise manner by applying volume perturbation incrementally during 16 seconds. The pressure signal was recorded and the pressure-volume (P-V) curve calculated from the plateau of each step. The constant K was obtained using the Salazar-Knowles equation and reflects the curvature of the upper portion of the deflation P-V curve. Quasi-static elastance reflects the static elastic recoil pressure of the lungs at a given lung volume. It was obtained by calculating the slope of the linear part of P-V curve.

After the measurements, the animals were sacrificed and bronchoalveolar lavage collected.

Histochemistry. The lungs were removed and formalin-fixed at a pressure of 25cm H_2O, paraffin-embedded and sectioned at 4μm thickness. Sagittal sections were used from each animal for histological and immunohistochemical assessment of damage, and morphometric analysis (mean linear intercept, Lm). Images from 10 fields per section were digitised using Image-Pro plus (version 5.1) and micropublisher 3.3 RTV camera connected to a Zeiss axioskope with 10x objective. The field size was 0.83 μm x 0.63 μm. Mean linear intercept was calculated from each field (horizontal and vertical) by dividing the length of the line by the number of alveolar intercepts.

Gordon and Sweet's Reticulin stain was performed as a method of visualising collagen distribution in both injured and vehicle-treated lung. Briefly, sections were oxidised with 0.5% potassium permanganate, bleached with 1% oxalic acid, and treated with 2.5% ammonium iron (III) sulphate and a 5% silver nitrate/1.5% sodium hydroxide solution prior to reduction with 10% unbuffered formaldehyde. Visualisation of reticulin fibres was accomplished via treatment with 0.1% sodium chloroaurate and 3% sodium thiosulphate solutions. Sections were counterstained with neutral red prior to mounting.

Image Processing and Stereological Analysis. Colour images of reticulin-stained sections were subjected to automated image processing methods developed in-house using Image Pro Plus (Media Cybernetics). Briefly, a greyscale image representing the green channel (which shows the highest differentiation from background) was obtained by splitting the RGB channels. Sobel edge detection operators, dilation-erosion and erosion-dilation algorithms were used to enhance the image and to remove 'salt and pepper' noise. An area of interest measuring 200μm x 200μm was overlaid over a digitally-captured image of a reticulin-stained section and only events completely inside the frame or intersecting the two inclusion edges of the frame's left and lower aspects (South-West) were included. Events intersecting the right and upper aspects (North-East) of the frame were excluded, as were blood vessels other than the capillaries of the alveolus. These stereological methods are similar to those described previously (Ochs et al., 2004). 2D objects that were counted using this method included alveolar septal junctions, free septal ends, and contiguous airspaces. A total of 15 non-overlapping frames were included per section as this was sufficient to achieve a running mean. The mean number of events on sections obtained from vehicle-treated (n=5), PPE-treated

(n=5), and JB1a-treated (n=5) mice were scored as a function of area (counts per 200μm x 200μm field of view).

Immunohistochemistry. Paraffin-embedded were deparaffinised, reydrated, and washed in water. For TTF-1 (clone 8G7G3/1, DAKO) immunohistochemistry, a microwave antigen retrieval method was used (3 x 5 minute 700W microwave treatments, in 10mM citrate buffer, pH 6.0). GATA-6 (H-92 rabbit polyclonal IgG, Santa Cruz) immunohistochemistry required proteinase K pretreatment (20μg/ml, 20 minutes, 37°C). Endogenous peroxidase activity was blocked with 3% hydrogen peroxide in water. Endogenous biotin was blocked with Avidin/Biotin Blocking Kit (Vector). Sections were blocked with either M.O.M IgG Blocking Reagent (Vector) or DAKO Protein Block Serum-Free (used for rabbit polyclonal antibodies) prior to incubation with primary antibody (diluted 1:50) overnight at 4°C. The following day, sections were washed 5 times in TBST (Tris-Buffered Saline pH 7.6, with 0.1% Tween 20) prior to incubation with biotinylated secondary antibody (30 minutes) and DAKO StreptABComplex/HRP (20 minutes). Immunohistochemical staining was visualised using DAB chromogen, a haematoxylin counterstain was used for sections other than those used to generate 3D reconstructions. Sections were washed, dehydrated and mounted in DPX. Negative controls omitted primary antibody step.

3D Reconstructions. 10 consecutive 3μm sections were used to generate 3D reconstructions of tissue parenchyma. Odd (1, 3, 5…) sections were labelled with GATA-6 whilst even (2, 4, 6…) sections were labelled with TTF-1. Digitally captured images were obtained with a QCapture Pro imaging system and a brightfield microscope (Zeiss Axioskop, 20x objective lens) and were patched into larger images

(3x3), which were interleaved to form their original order in an image stack prior to alignment using Adobe Photoshop 7.0.1. TIFF images were cropped, resized (6000x6000 pixels) and image stacks were imported into Amira 4.0 for isosurface rendering, which was accomplished at threshold values sufficient to detect either immunohistochemical label or tissue parenchyma. Isosurfaces were coloured either red (TTF-1), blue (parenchyma) or yellow (GATA-6) for enhanced visualisation.

Apoptosis measurement. Terminal Deoxyribonucleotidyl Transferase (TdT)-Mediated dUTP Nick End Labelling (TUNEL) was assessed in sections using the Red ApopTagTM Kit (Chemicon). Data for the quantification of positively stained apoptotic nuclei was acquired using the x40 oil objective of a Zeiss 510 Axiovert confocal microscope system (Carl Zeiss Ltd, UK). The stage-tiling utility was employed for the collection of 4x4 tiled images, equivalent to a total area of 0.921mm x 0.921mm, imaged from a lung section of ~8mm x 8mm (two tiles each from right and left lobes). Images of mainly alveolar tissue were constructed. The images were then converted to 8-bits grey scale and ImageJ was used to count total number of cells. TUNEL positive cells were counted manually.

Human mesenchyme and epithelial cell co-culture *in vitro*. Adult human lung fibroblasts (CCD-8Lu) were seeded onto collagen I coated BioFlex 6 well plates at 0.5 X 10^6/well. The following day, NCI-H441 were seeded on top of the fibroblasts at the same density. NCI-H441 cells possesses alveolar type II cell characteristics. Cells were starved with media containing 0.1% FCS. The plates were subjected to stretching at 0-5%, 0-10% or 2-10% sinusoidal stretch at 1Hz for 6 hours. Control plates on plastic or bioflex plates without stretch were also included. PPE was added at 0.06 or 0.3U/ml

alone or in combination with JB1a (2μg/ml) and ZVAD-fmk at 10 or 20 μM. At the end of the 6 hour period, the media was aspirated and caspase 3 activity assayed using Caspase-Glo^{TM} 3/7 (Promega) according to the manufacturers' instructions. Separate experiments were performed at up to 6 hours of stretching where the cells were fixed with 4% paraformaldehyde and stained using Alexa-fluor phalloidin and TO-PRO3 (Molecular Probes). Images were aquired using Zeiss Axioskope using a x63 water achroplan objective and analysed using LSM 5 Image software.

In a separate set of experiments lung fibroblasts and epithelial cells were seeded onto 96 multi-well plates as described above. The cells were starved in media containing 0.1% FCS then in DMEM-glucose-free with 0.1% FCS for 45 minutes before treating with (i) PPE at 0.3U/ml alone or (ii) PPE preceded by JB1a (2μg/ml). At the end of the experiment, ATP levels were measured using a bioluminescent ATP kit (Perkin Elmer).

Time-lapse studies. Cells were cultured as described in methods at 50,000 cell/membrane onto collagen I Bioflex membranes using silicone gaskets of 10mm diameter. Cells were starved with media contaning 0.1% FCS and Syto 16 (Molecular Probes). The media was removed and Alexa-Fluor 647 labelled G-actin from rabbit (100μg/membrane) was loaded using Influx (Molecular Probes). The cells were loaded with PhiPhiLux-G_2D_2 for visualisation of caspase activation (OncoImmune). The membrane was then mounted onto the StageFlexer (FlexCell), placed on the stage of an upright Leica-TCS-NT confocal microscope system (Leica Microsystems GmbH, Germany) and subjected to 2-10% cyclic stretch at 1 Hz for up to 6 hours. Images were collected simultaneously from 3 channels at 1 minute intervals, using the x10 lens. The resulting timelapse movies were collated and analysed with Imaris software (Bitplane

AG, Switzerland). At various time points during the study, the membrane was held static while serial optical sections were acquired. The three fluorescent channels supplemented by the collection of the brightfield channel image.

Three-dimensional confocal microspy. NCI-H441 cells and human lung fibroblasts were cultured as described above onto collagen I-coated glass coverslips at 20,000 cells within an area of 5mm in diameter. The media was removed and Alexa-Fluor 647 labelled G-actin (30μg/coverslip) from rabbit was loaded using Influx (Molecular Probes). The cells were loaded with PhiPhiLux-G_2D_2 for visualisation of caspase activation (OncoImmune) and FL-ganglioside 1 (GM1, Molecular probes) to visualise the plasma membrane. Images were collected through 4 separate channels (GM1: λ = 488 ,caspase λ = 568, actin: λ = 647 and brightfield) using x63 water lens and Zeiss LSM510 CLSM microscope. The resulting images were analysed with Imaris software (Bitplane AG, Switzerland). Three-dimensional images were reconstructed.

Caveolin-1 extraction and analyses. NCI-H441 cells and human lung fibroblasts were cultured as described above. Media was changed prior to the experiment to 0.1% FCS containing media. Vehicle, PPE (0.3U/ml) or PPE in the presence of JB1a (2 μg/ml) containing media was added onto the cells for 2 hours. Cells were extracted using lysis buffer composed of 50 mM Tris-HCl (pH 7.5), 1 mM EDTA, 1 mM Na3VO4 containing 1% Triton X-100 and protease inhibitors (Roche) for 1 hour at 4^{o}C and sheared repeatedly using 22G needle on ice. Total protein was quantified using Bradford's assay method (BioRad). The extracts (1ml) were mixed with equal volume of 85% w/v sucrose in extraction buffer without Triton x-100 and layered with 2ml of 35% w/v sucrose in buffer and then 1 ml of 5% w/v sucrose in buffer. The gradients

were prepared at 4°C. The gradients were then centrifuged at 38,000 rpm for 16 hours at 4°C. Fraction were collected from the top (0.4 ml fractions) and separated onto 13% SDS-PAGE and transferred onto nitrocellulose membranes then probed for β1 integrin using JB1a (Chemicon), caveolin-1 (BD Biosciences), phosphorylated caveolin-1 (Cell Biosciences) and talin (Sigma-Aldrich), and developed with HRP-conjugated secondary antibodies using the ECL-plus chemiluminescence system (Amersham Biosciences).

Figure 1

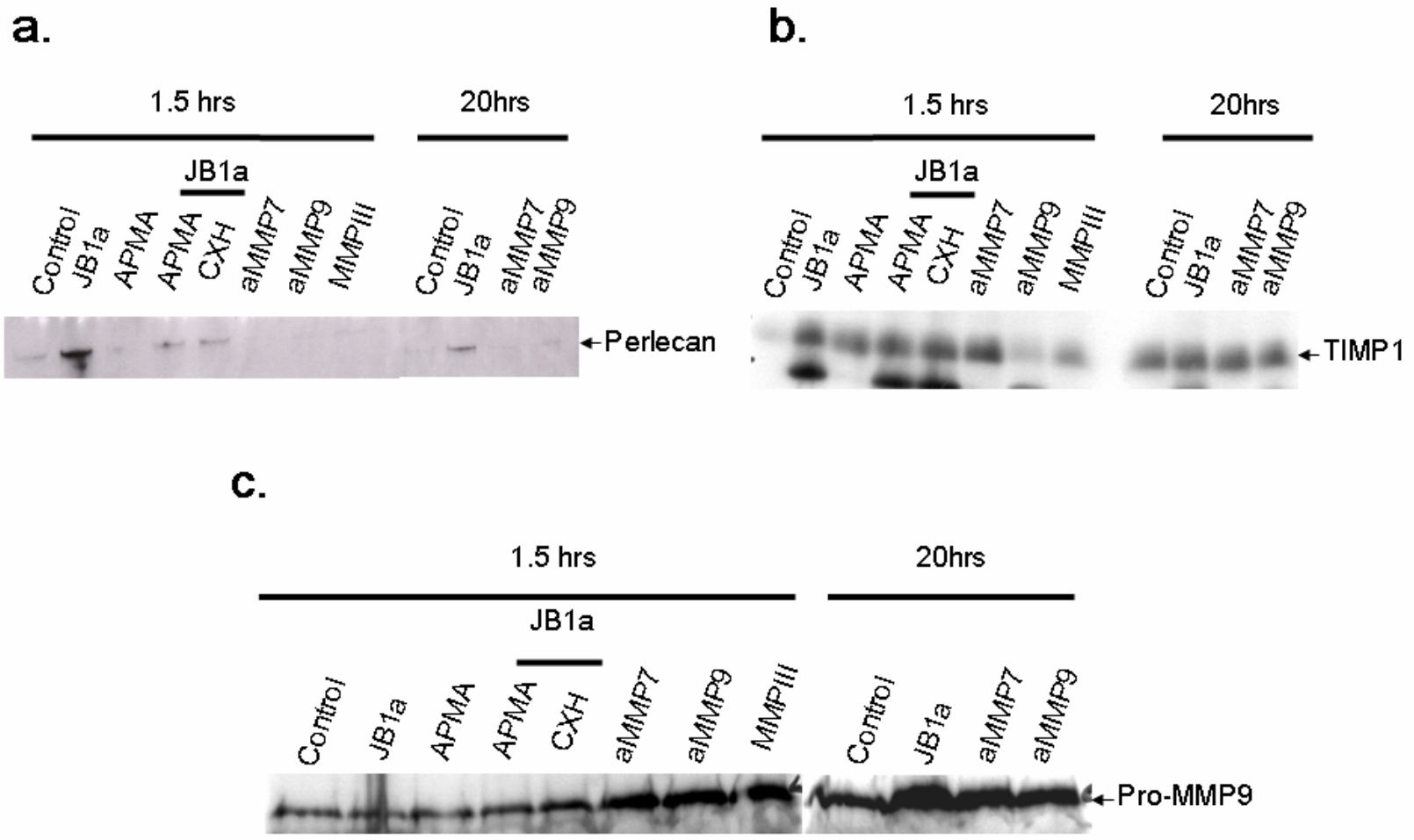
a.
1.5 hrs
20hrs
JB1a
Control
JB1a
APMA
APMA
CXH
aMMP7
aMMP9
MMPIII
Control
JB1a
aMMP7
aMMP9
Perlecan
b.
1.5 hrs
20hrs
JB1a
Control
JB1a
APMA
APMA
CXH
aMMP7
aMMP9
MMPIII
Control
JB1a
aMMP7
aMMP9
TIMP1
c.
1.5 hrs
20hrs
JB1a
Control
JB1a
APMA
APMA
CXH
aMMP7
aMMP9
MMPIII
Control
JB1a
aMMP7
aMMP9
Pro-MMP9

Figure 2

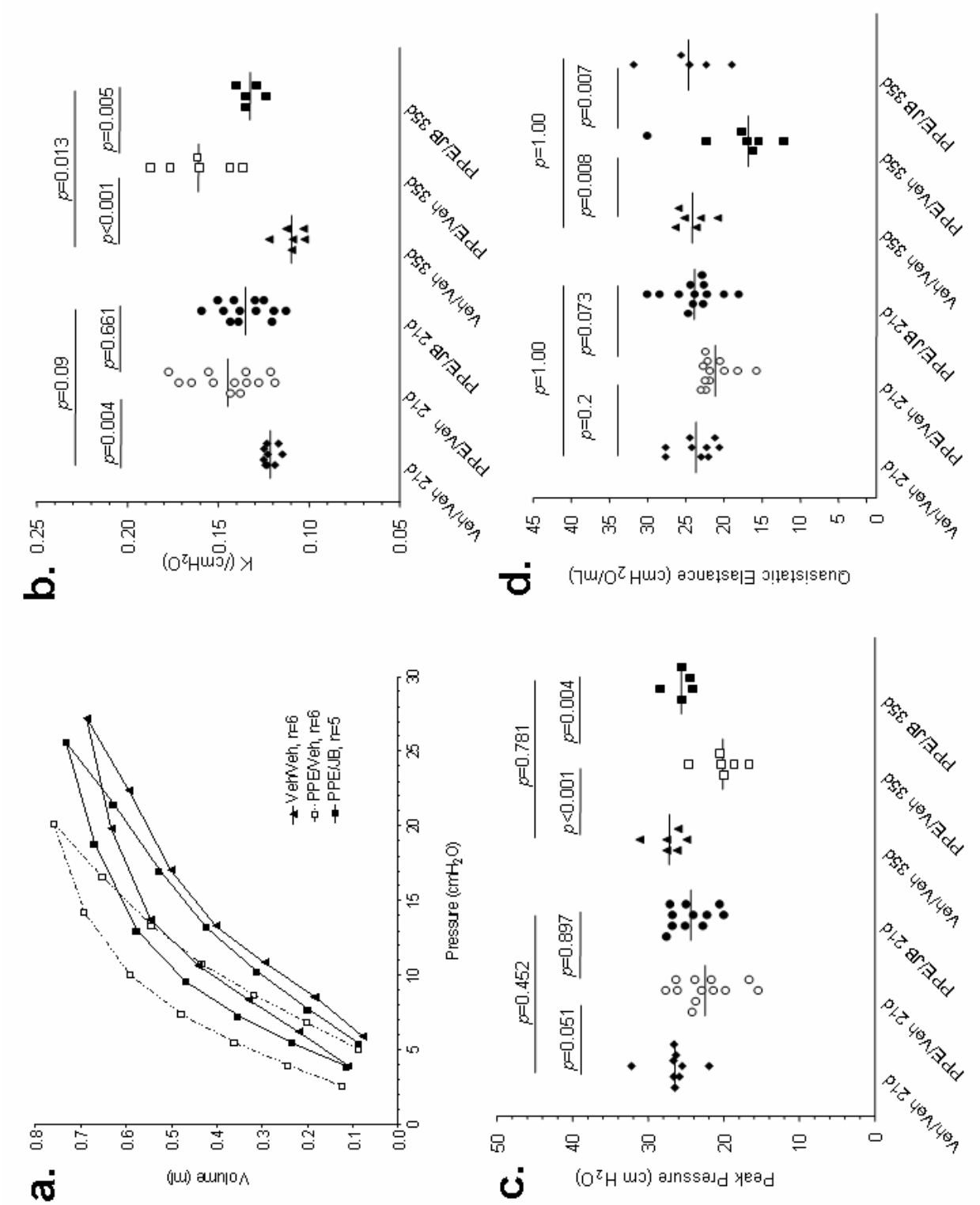

Figure 3

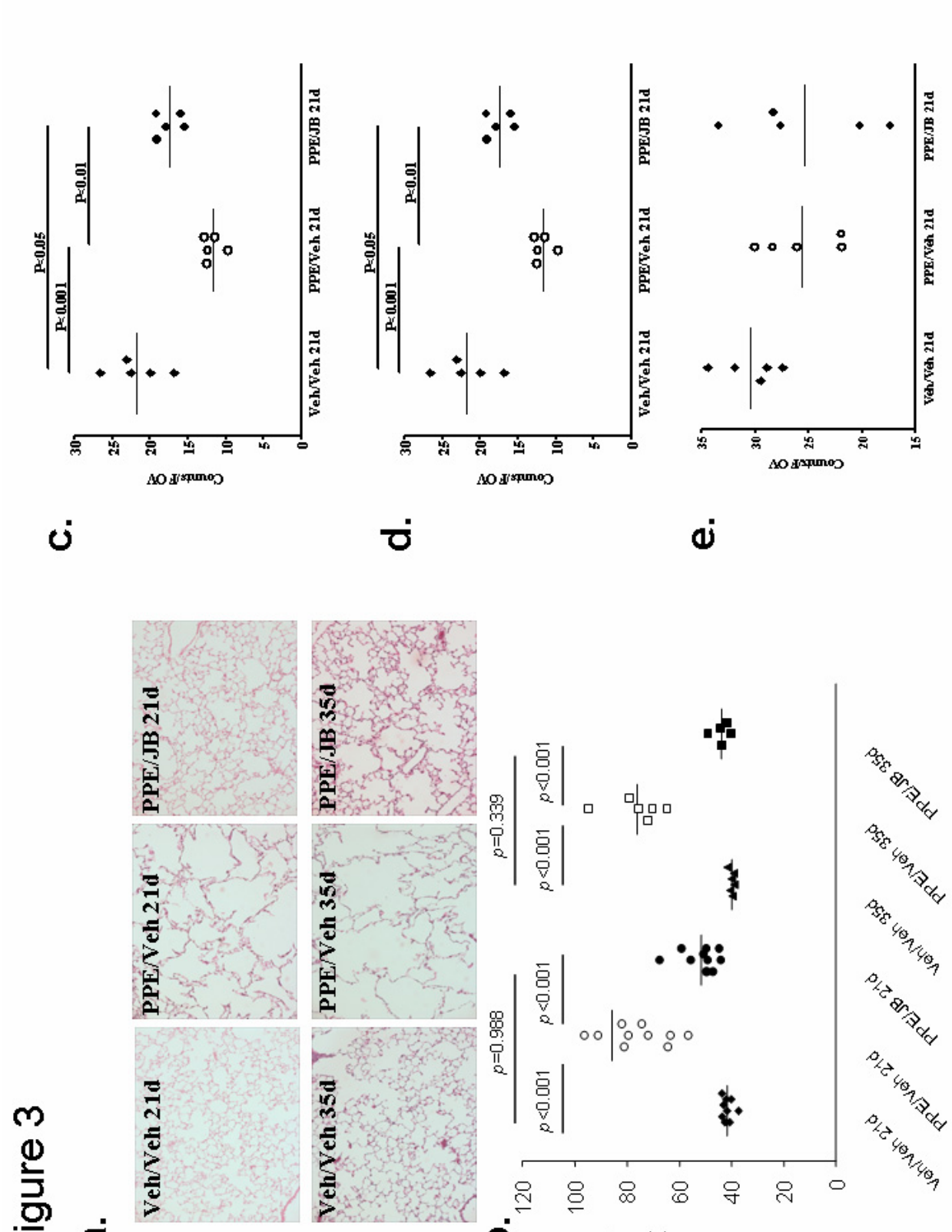

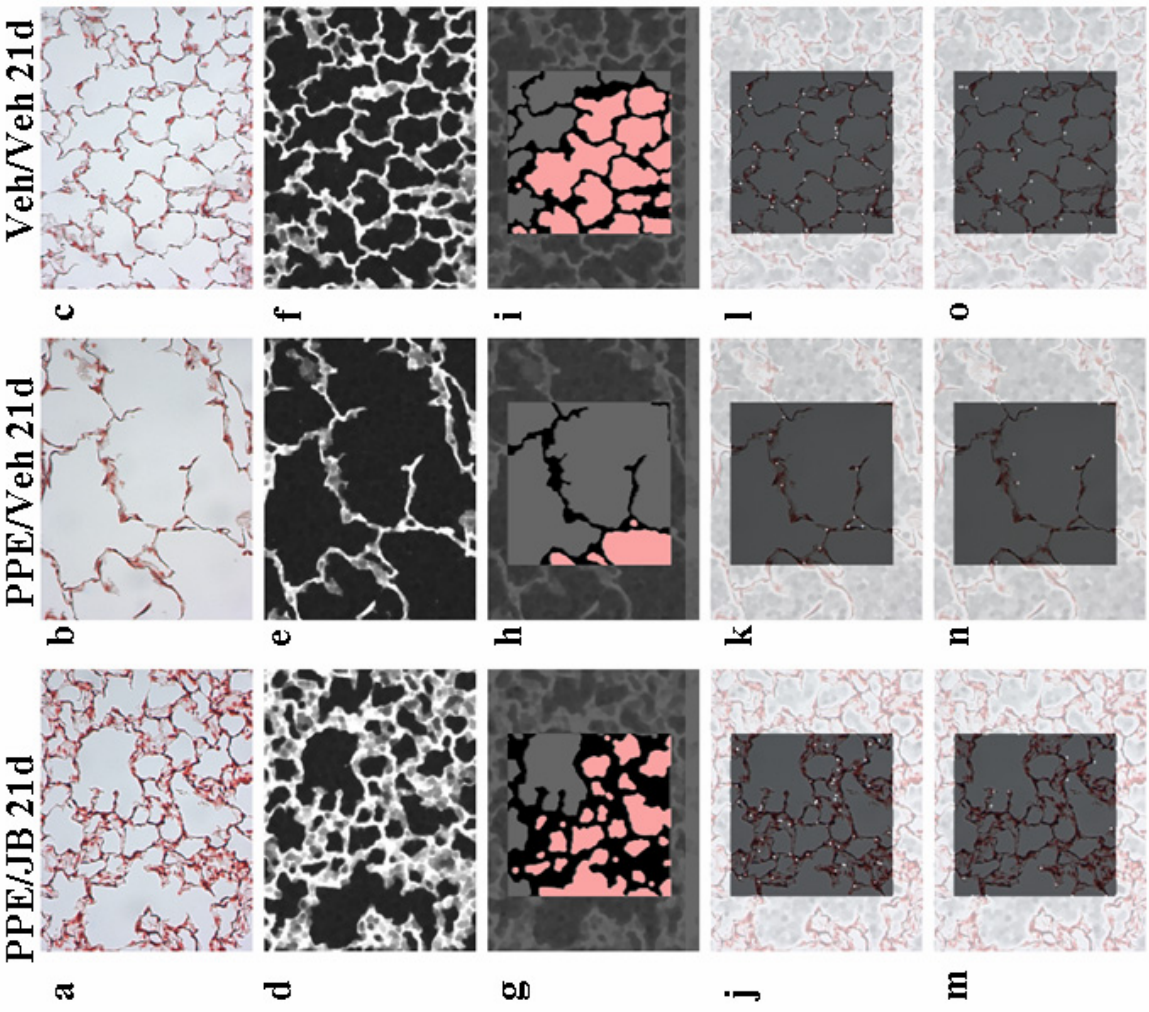

Figure 4

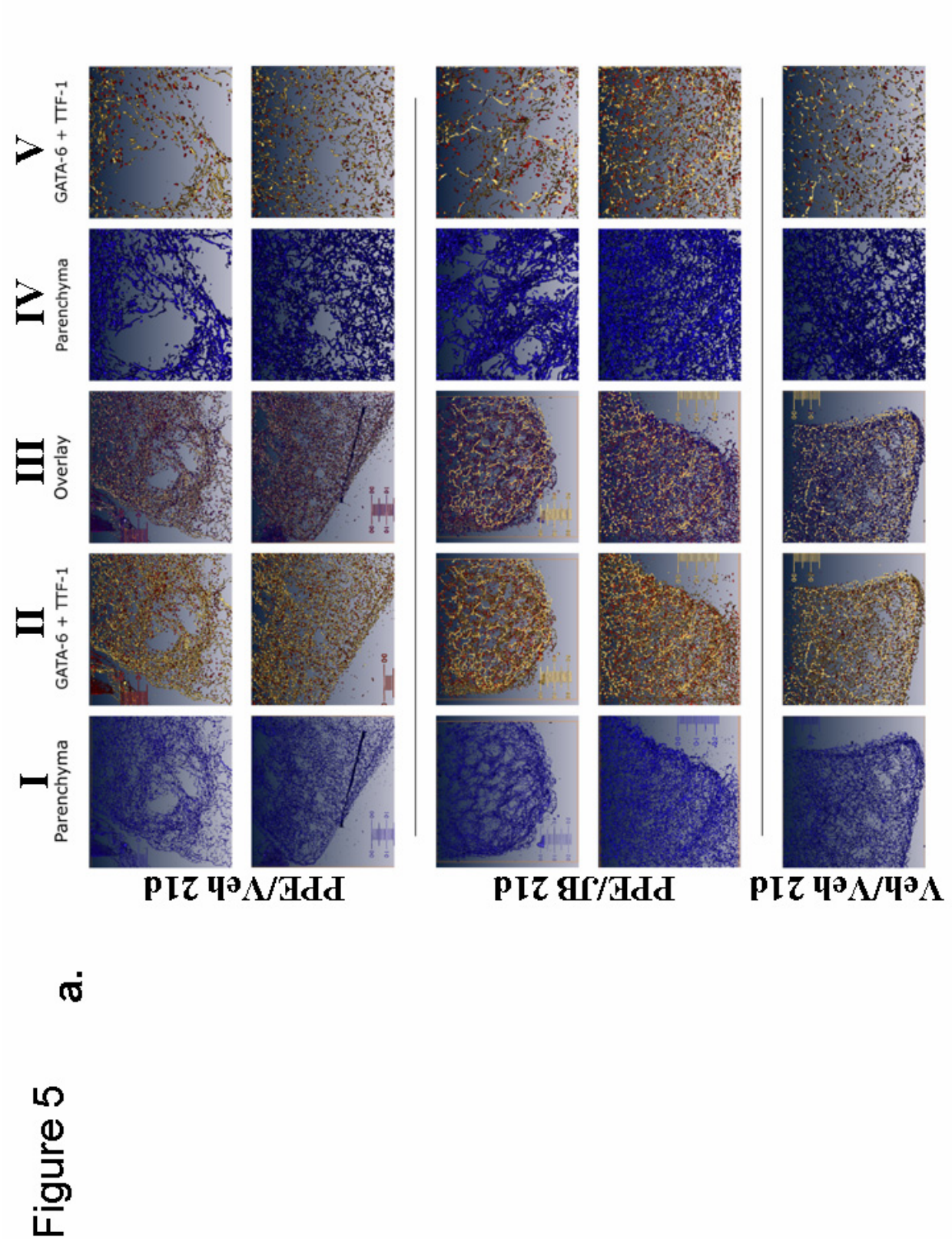

Figure 5

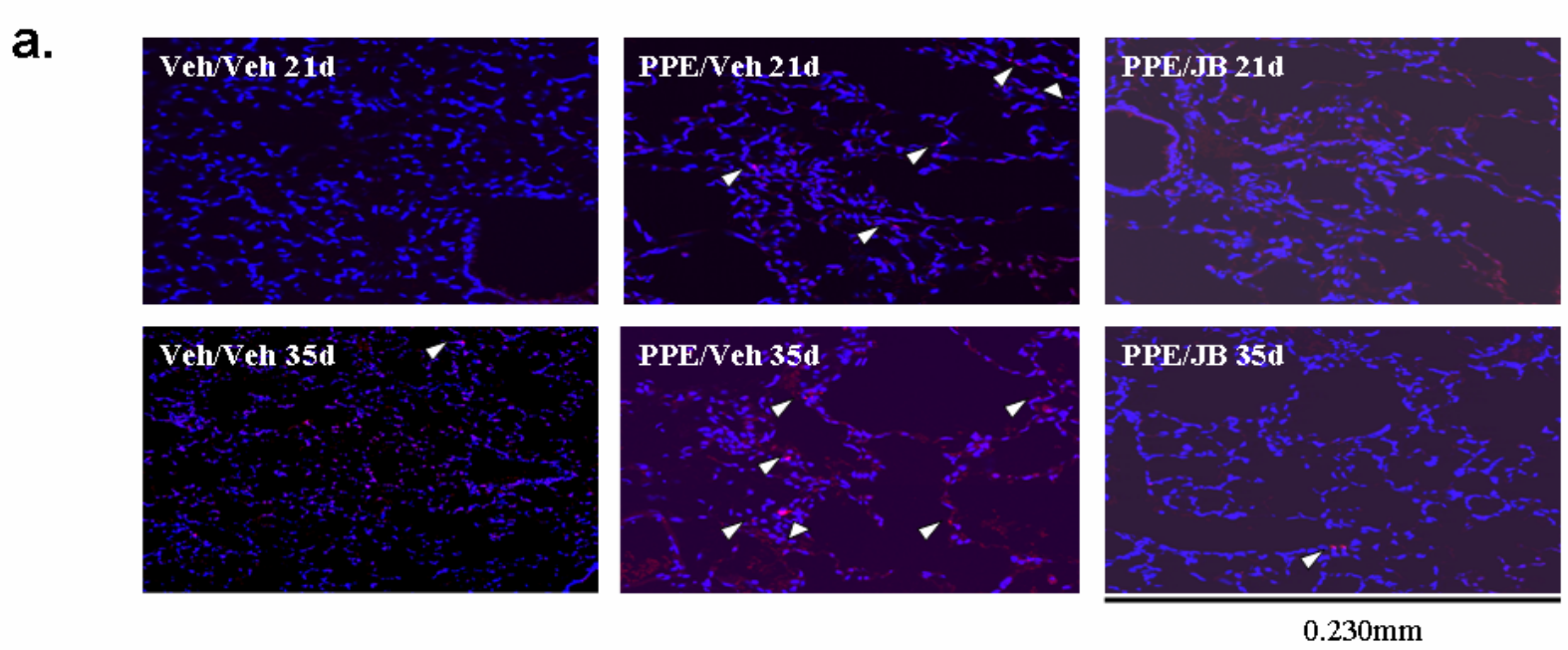
a.
Veh/Veh 21d
PPE/Veh 21d
PPE/JB 21d
Veh/Veh 35d
PPE/Veh 35d
PPE/JB 35d
0.230mm
b.
% TUNEL positive cells
6.0
5.5
5.0
4.5
4.0
3.5
3.0
2.5
2.0
1.5
1.0
0.5
0.0
P<0.05
P<0.05
P<0.05
P<0.05
Veh/Veh21d
PPE/Veh21d
PPE/JB21d
Veh/Veh35d
PPE/Veh35d
PPE/JB35d

Figure 6

Figure 7

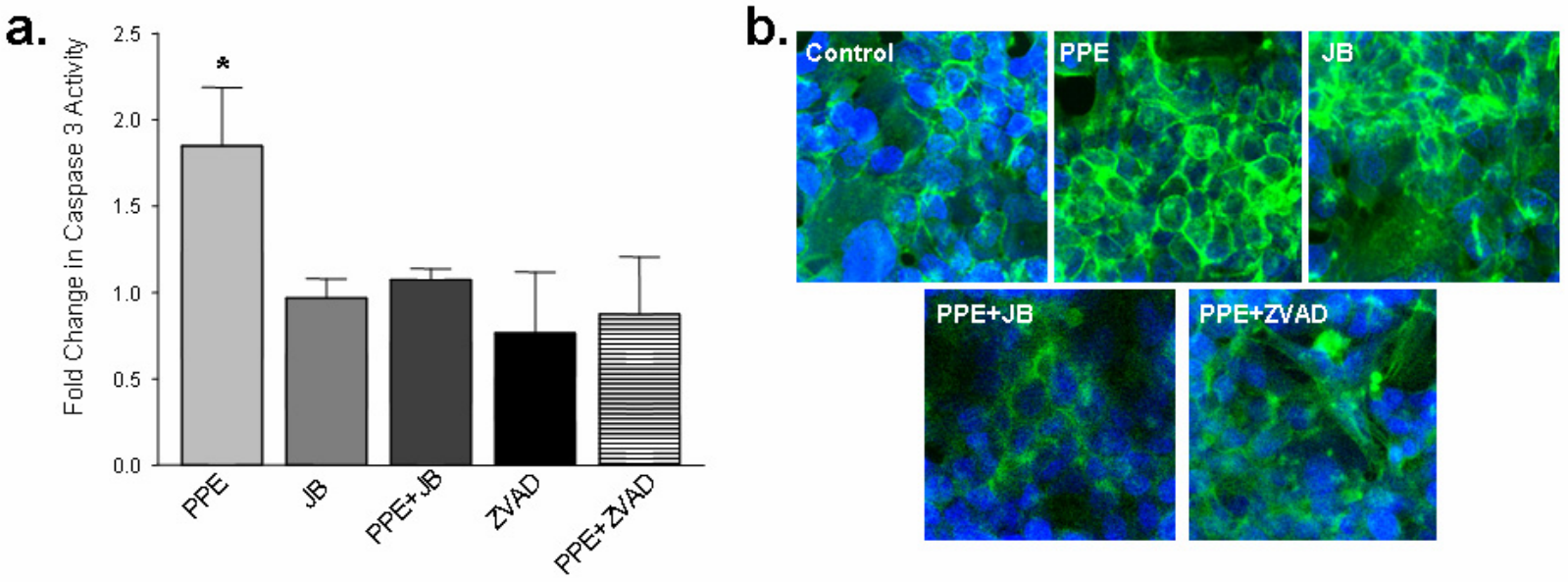
a.
Fold Change in Caspase 3 Activity
2.5
2.0
1.5
1.0
0.5
0.0
*
PPE
JB
PPE+JB
ZVAD
PPE+ZVAD
b.
Control
PPE
JB
PPE+JB
PPE+ZVAD

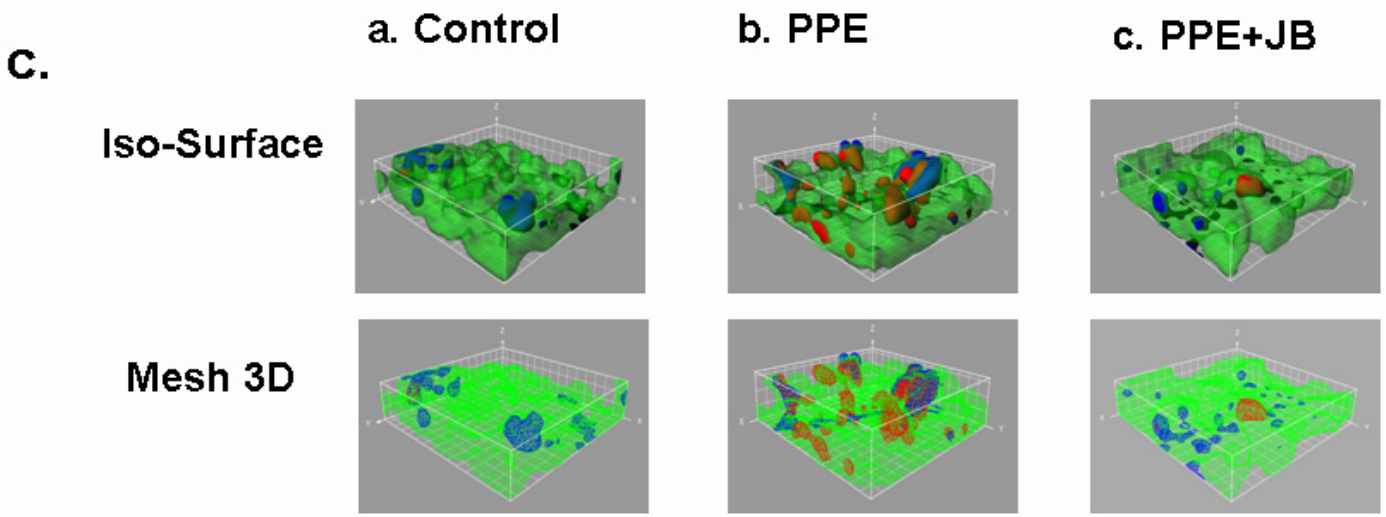
c.
a. Control
b. PPE
c. PPE+JB
Iso-Surface
Mesh 3D

Figure 8

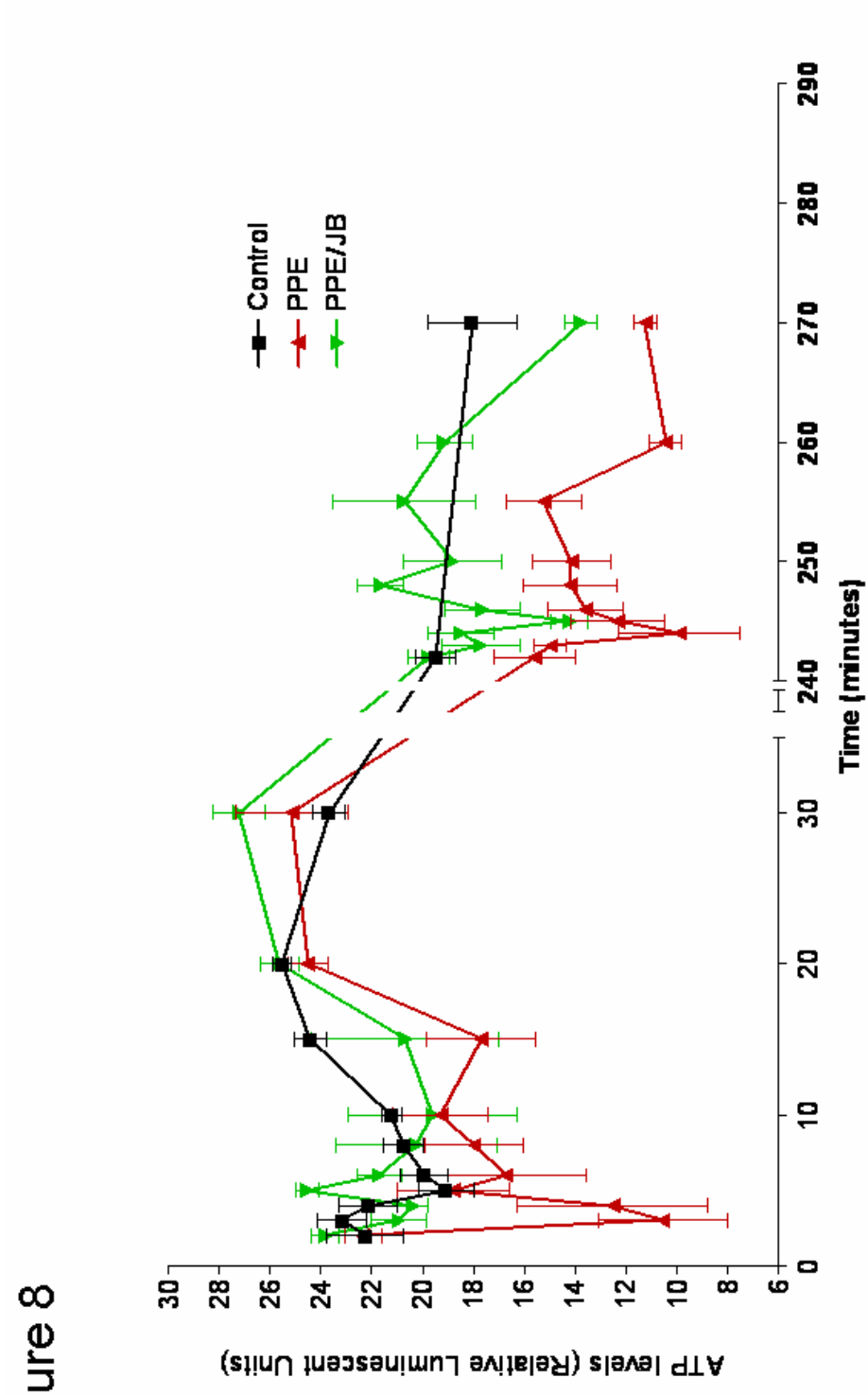

Figure 9

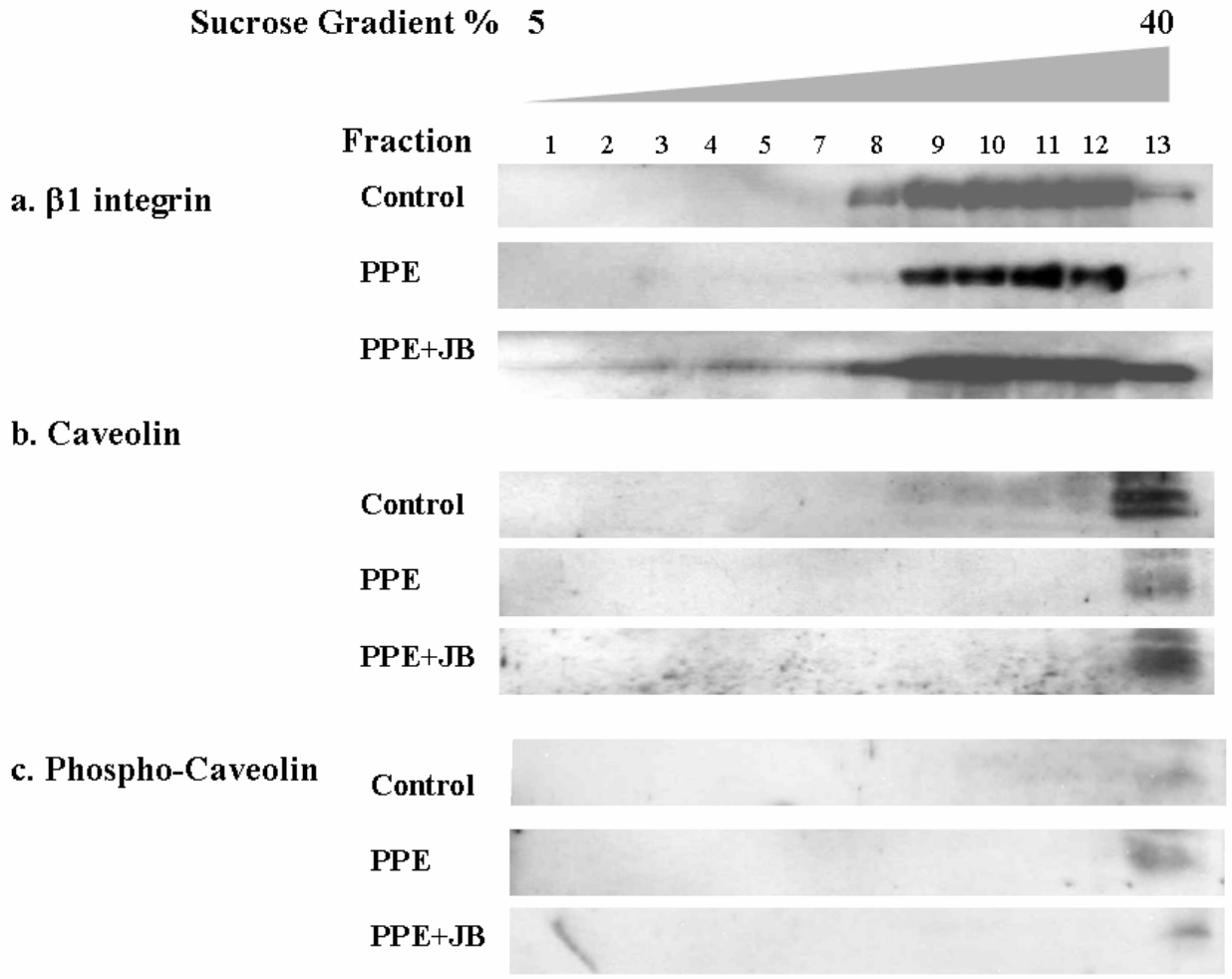
Sucrose Gradient % 5
40
Fraction
1 2 3 4 5 7 8 9 10 11 12 13
a. β1 integrin
Control
PPE
PPE+JB
b. Caveolin
Control
PPE
PPE+JB
c. Phospho-Caveolin
Control
PPE
PPE+JB

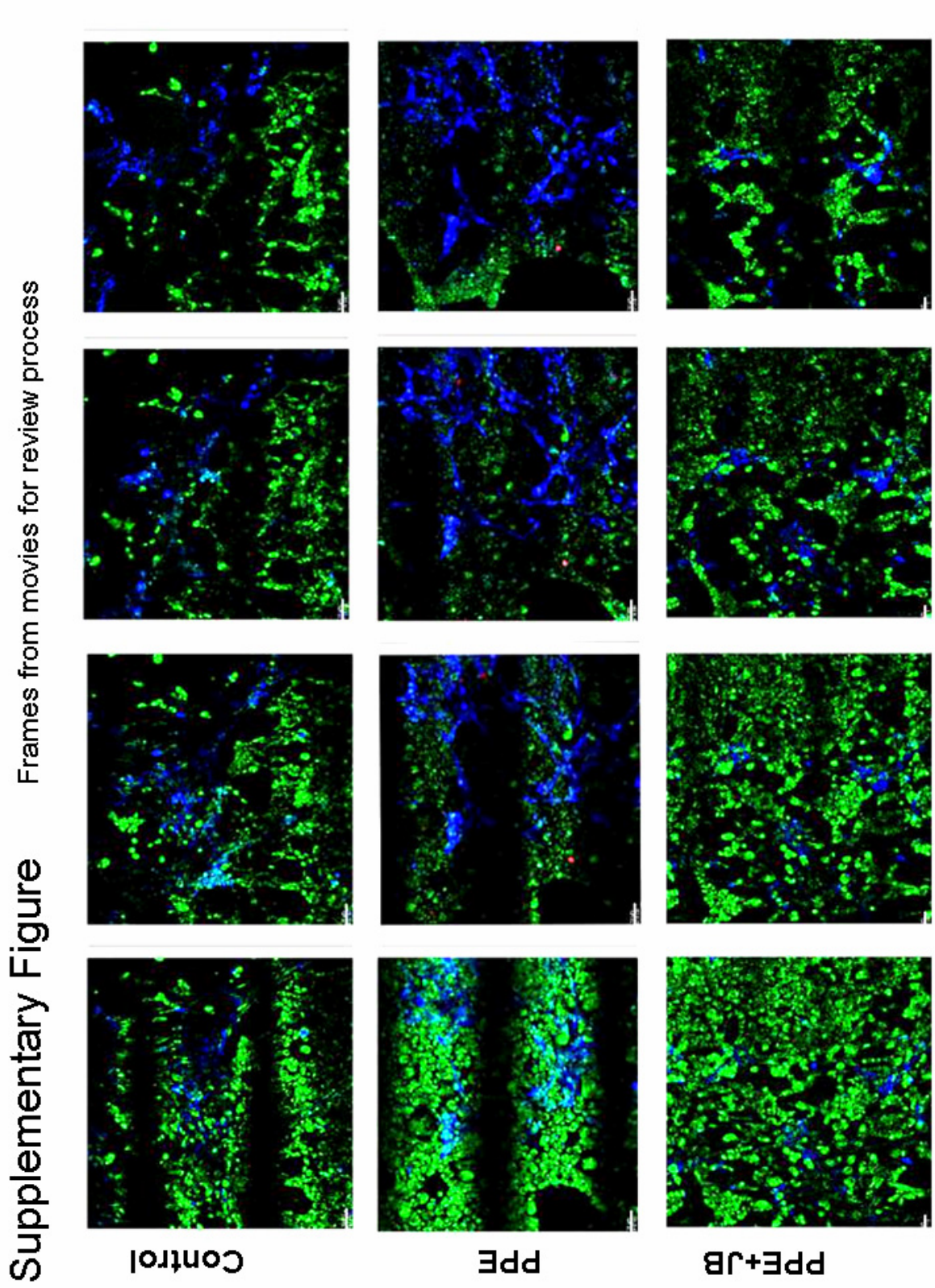

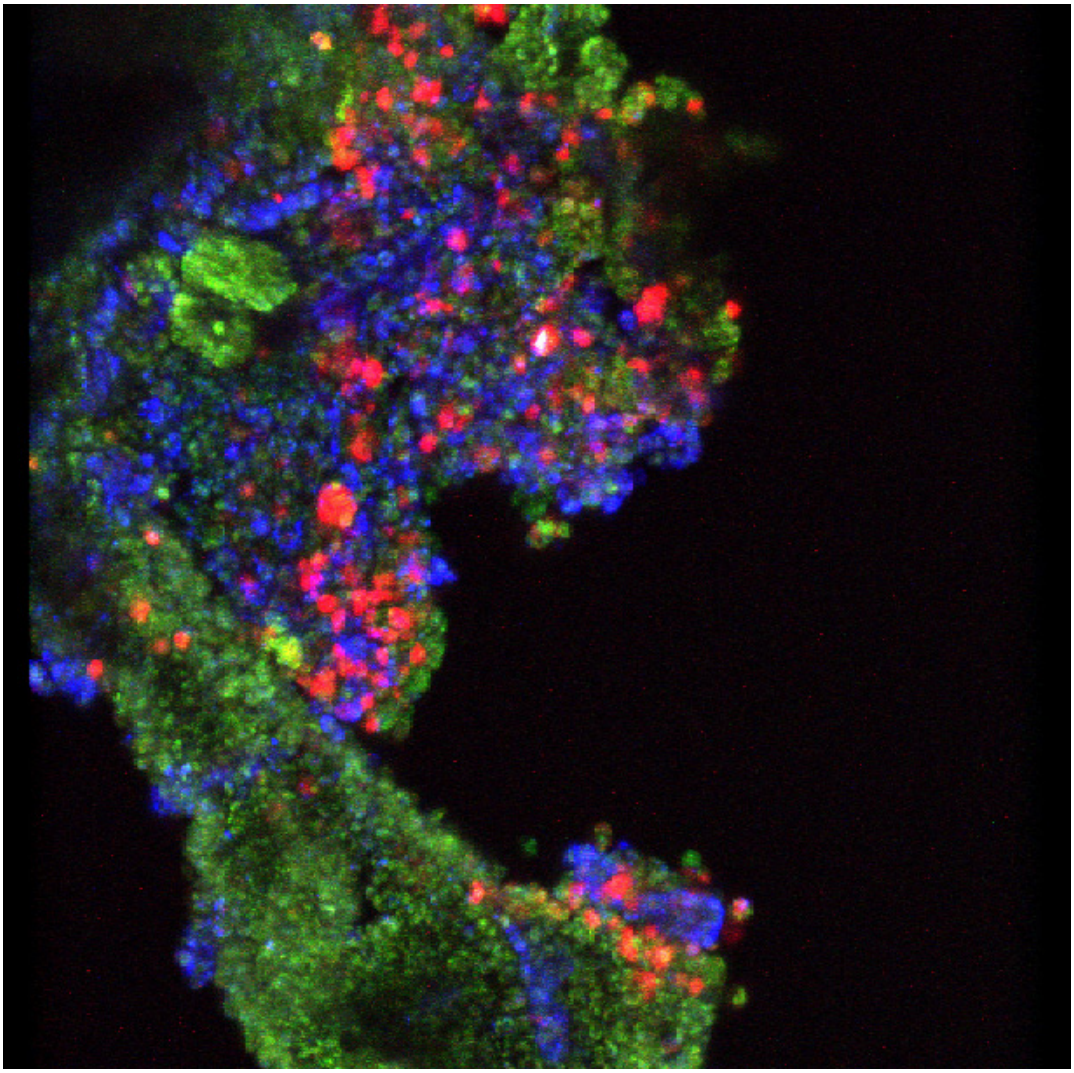

Supplementary Figure. An image which highlights the peak activation of caspase (red) following elastase-induced injury in vitro, and its presence in high actin aggregate-containing (blue) cell populations.